Performance of third-order ghost imaging with second-order intensity correlation

Bin Cao (曹 彬)*, Chunxi Zhang (张春熹), and Pan Ou (欧 攀)

School of Instrumentation Science and Opto-Electronics Engineering, Beihang University, Beijing 100191, China

**Corresponding author: cao_bb@hotmail.com*

Received November 16, 2010; accepted March 15, 2011; posted online May 31, 2011

The third-order ghost imaging with the second-order intensity correlation is theoretically and experimentally demonstrated. The resolution and visibility of the reconstructed image are discussed, and the relationship between resolution and visibility is analyzed. The theoretical results show that a tradeoff exists between the visibility and resolution of the reconstructed image; the better the image resolution, the worse the image visibility. Numerical simulations are carried out to verify this theory, and a ghost imaging experiment is conducted to validate our calculations. The experimental results agree with the theoretical predictions.

OCIS codes: 100.4994, 110.2960.
doi: 10.3788/COL201109.081102.

Correlated imaging, also known as "intensity correlation", was first introduced by Hanbury Brown *et al.* in 1956[1]. The principle of correlated optical imaging is based on classical and quantum coherent theory[2]. Ghost imaging and ghost diffraction are typical practical applications of optical intensity correlation[3−19].

Ghost imaging, proposed in 1995[6], is a novel imaging method that indirectly retrieves information about an unknown object. In the principal setup of the second-order ghost imaging, the seminal light beam is split into two separated daughter beams that are spatially correlated. Each of the correlated beams passes through a different imaging system. One beam path, usually called the "test arm", is sent through an unknown object and detected by a bucket detector that collects all the incoming light. Meanwhile, the other one that travels in a specific path called the "reference arm", is detected by a scanning point-like detector on the transverse plane. The object can be reconstructed from the spatial cross-correlation between the intensity fluctuations of the two detectors. The correlogram indicates the object image.

The bottleneck of the second-order ghost imaging in which a fully incoherent light source is used lies in low visibility, which never exceeds 33.3%[16]. Visibility can be enhanced with a high-order intensity correlation[16−18]. In the principal setup of the high-order ghost imaging, the light source is split into several separated light paths and detected by N detectors[15]. Cao *et al.*[17] proposed that a high-order intensity correlation can be implemented by two detectors, i.e., one intensity is composed of an n-fold intensity product and the other intensity is an $(N-n)$-fold product.

In this letter, the third-order ghost imaging is realized using two detectors with a fully incoherent light source. The resolution and visibility of the obtained image are influenced by the optical transverse coherent length at the object. A comparison of the second-order and third-order ghost imaging shows that both yield the same resolution; however, the visibility in the third-order ghost imaging is higher than that in the second-order ghost imaging when their optical transverse coherent lengths are equal. In addition, a tradeoff between the resolution and visibility of the third-order ghost imaging continues to exist, similar to that observed in the second-order ghost imaging. To validate our theoretical analysis, a novel ghost imaging experimental configuration is proposed and investigated. With the proposed ghost imaging experimental setup, any arbitrary-order ghost imaging can be realized, and its resolution and visibility can be adjusted conveniently.

To exploit the properties of the third-order ghost imaging performed with the second-order intensity correlation, the setup depicted in Fig. 1 is considered. The imaging system uses a fully incoherent light as light source. The incoherent light beam is split into two spatially correlated daughter light beams by a beam splitter. The two daughter light beams propagate in the test arm and reference arm, as previously mentioned. An unknown object is placed in the test arm and a bucket detector is located immediately after the object, so that all the light passing through the object is collected. The other daughter beam, which travels through the reference arm, is detected by a scanning point-like detector. Both the bucket detector and the point-like detector are located in the optical far field of the light source. Then, the optical intensity correlation is measured using an intensity correlation calculation system. The two detectors are spatially resolved; hence, the second-order intensity correlation function is registered as a function of the position of the two detectors. By scanning the point-like detector, the image of the object can be reconstructed.

A detailed theoretical analysis of the third-order ghost imaging is necessary. For simplicity, only a one-dimensional case is considered in the following analysis. According to Ref. [15] and the experimental configuration shown in Fig. 1, the third-order ghost imaging function can be expressed as

$$g^{(3)}(x_1,x_2) = 2 + \frac{4}{l_{\rm o}}\int\limits_{x_2} |t(x_2)|^2 \sin {\rm c}^2\Big[\frac{\pi(x_1-x_2)}{l_{\rm c}}\Big]{\rm d}x_2, \tag{1}$$

where $l_{\rm o}$ is the transversal transmission light size of the imaged object; $l_{\rm c}$ is the optical transverse coherent length on the detection plane defined as $l_{\rm c} = \lambda z/l_{\rm s}$[19], with $l_{\rm s}$ as the transverse size of the light source; z is

 © 2011 Chinese Optics Letters

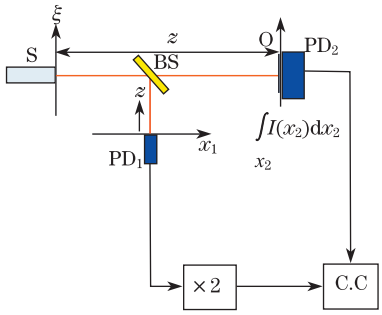

Fig. 1. Schematic of a third-order ghost imaging system based on the second-order intensity correlation. S stands for the incoherent light source; BS is the beam splitter; PD_1 indicates a point-like detector; PD_2 stands for the bucket detector; O stands for an unknown object; C.C stands for correlation calculation. In the third-order ghost imaging scheme, the intensity of PD_1 is calculated twice in calculating intensity correlation.

the distance between the light source and detectors; λ is the wavelength of the light source.

The first term on the right-hand side of Eq. (1) is the direct current (DC) background, which does not contain any image information. Conversely, the second term consists of information on the unknown object as the transmission function of the unknown object $t(x_2)$ is included. As a result, the spatial information on the object can be retrieved, but the phase information is lost. In what follows, the resolution and visibility of the third-order ghost imaging calculated by the second-order intensity correlations are discussed.

Equation (1) shows that when $l_c \to \infty$, the sinc function approaches constant 1; hence, $g^{(3)}(x_1, x_2)$ changes slowly and no information on the object image can be retrieved. On the other hand, when $l_c \to 0$, the sinc function approaches δ-function; therefore, $g^{(3)}(x_1, x_2)$ varies dramatically as variable x_1 is scanned, and the spatial information on the image can be obtained. Consequently, the resolution of the ghost imaging increases with the reduction of l_c, and vice versa.

Let us now consider the visibility of the third-order ghost imaging. Assuming that the transversal transmission light size of the object does not change, Eq. (1) shows that $g^{(3)}(x_1, x_2)_{\min}$ always equals DC component 2. As for $g^{(3)}(x_1, x_2)_{\max}$, when $l_c \to \infty$, $g^{(3)}(x_1, x_2)_{\max} = 6$; thus, the maximal visibility is 50%. When $l_c \to 0$, $g^{(3)}(x_1, x_2, x_3)_{\max} = 2$, the visibility becomes zero. The visibility of the third-order ghost imaging is proportional to l_c, and vice versa.

From the foregoing discussion, we can determine that the resolution of the third-order ghost imaging increases with decreasing l_c, and the visibility increases with the increment in l_c. Similar to that observed in the second-order ghost imaging, the tradeoff between resolution and visibility in the third-order ghost imaging using a second-order intensity correlation continues to exist.

In contrast to the third-order ghost imaging, the second-order ghost imaging function is expressed as

$$g^{(2)}(x_1, x_2) = 1 + \frac{1}{l_o} \int_{x_2} |t(x_2)|^2 \operatorname{sinc}^2\left[\frac{\pi(x_1 - x_2)}{l_c}\right] \mathrm{d}x_2. \quad (2)$$

Comparing Eqs. (1) and (2) reveals that because of the same integrands in both second items, the second- and third-order ghost imaging that are realized with a second-order intensity correlation have the same resolution capacity. However, the visibility is influenced by the DC background and the coefficient of the second item.

A double-slit is used as the imaged object, and numerical simulations are performed to investigate the properties of the reconstructed image. Reconsidering the experimental setup depicted in Fig. 1, a fully incoherent light source is used and a double-slit O is placed immediately before the bucket detector. The slit width of the double-slit is $w = 0.2$ mm and the distance between two slits is $d = 0.3$ mm. Therefore, the transmission function of the object $t(x_2)$ can be expressed as $t(x_2) = 1$ if -0.35 mm $\leqslant x_2 \leqslant -0.15$ mm and 0.15 mm $\leqslant x_2 \leqslant 0.35$ mm; otherwise, $t(x_2) = 0$.

The numerical simulation results are shown in Fig. 2, where Figs. 2(a) and (b) show the images that are reshaped by the second- and third-order ghost imaging under different specific optical transverse coherent lengths l_c on the detection plane. For both the second- and third-order ghost imaging, the quality of the image improves when l_c decreases. Hence, the image resolution for both methods is inversely proportional to l_c, a result that agrees with the theoretical predictions. Figure 2(c) shows that the visibilities of the second- and third-order ghost imaging change at several values of l_c. The visibility of the third-order ghost imaging increases when l_c increases, which is also consistent with the theoretical predictions. Furthermore, the visibility of the third-order ghost imaging is better than that of the second-order ghost imaging when the optical transverse coherent lengths of both are equal. These numerical analysis results show that the tradeoff between the resolution and visibility of the third-order ghost imaging by the second-order intensity correlation continues to exist.

We conduct a novel experimental scheme (Fig. 3) to verify the foregoing theory. An erbium-doped fiber amplifier (EDFA) is used as the light source without employing an optical input signal. Both the forward and backward pumps are used so that the EDFA emits approximately 27 mW of amplified spontaneous emission light at λ=1.55 μm. The fiber-coupled output of the EDFA and the outgoing light are collimated with an adjustable lens (L_1). A rotating ground glass is placed in the beam path after lens L_1, thereby producing a spatially incoherent beam. The laser diameter incident on the ground glass can be modified by adjusting lens L_1. The diffused beam is divided into two independent daughter beams with a 50/50 beam splitter, creating two identical speckle patterns. The transmitted part of the beam that is transmitted through the beam splitter is the test arm, and the reflected part of the beam is the reference arm. A double-slit located approximately 100 mm from the ground glass is placed in the test arm, and the light beam is transmitted through the object. A fixed lens L_2 is placed immediately after the double-slit, and the light is collimated into a multimode fiber of 62.5 μm core diameter. The combined lens L_2 and multimode fiber play the role of a bucket detector. A single-mode fiber with a 10-μm core diameter is placed in the reference arm; it is mounted on an *xyz* translation stage.

The single-mode fiber is scanned at a step of 20 μm across the diffuse beam diameter over the transverse plane, and the correlation is measured at many points across the scanning process. The output from each fiber is independently detected by a photodiode (818-IR, Newport, USA) and sent to an oscilloscope (TDS 724D, Tektronix, USA) with a 500-MHz bandwidth. The optical paths of the two imaging systems are arranged so that they are approximately equal. The data are acquired at an exposure time of 0.1 ms, much shorter than the correlation time of the light source. The data are then transmitted through a general purpose interface bus (GPIB) cable and saved in a computer.

The experimental results with different laser diameters incident on the ground glass are shown in Fig. 4. The complete scanning results reveal that the image of the double-slit and the full-width at half-maximum (FWHM) is 0.2 mm, and that the distance between the two slits is 0.3 mm, which is in agreement with the original image. The visibilities of the reconstructed patterns are 7% and 14.9% corresponding to the l_s of 2.5 and 1 mm; the resolution of the image obtained when l_s=2.5 mm is better than that when l_s=1 mm. Therefore, the larger the diameter of the laser spot on the ground glass, the lower the visibility and the better the resolution, and vice versa[12]. These results are in good agreement with the theoretical and numerical predictions.

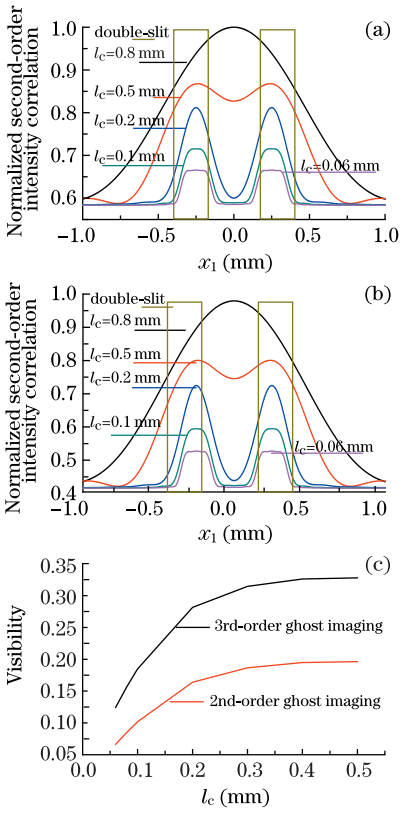

Fig. 2. Reshaped images obtained in numerical simulations by (a) the second-order and (b) the third-order ghost imaging under different specified values of l_c. For a double-slit, the slit width is 0.2 mm, the distance of two slits is 0.3 mm, and the distance between double slits and the ground glass is 20 mm. All curves are normalized by the maximal intensity correlation value when l_c = 0.8 mm. (c) Dependence of the visibility of the second- and third-order ghost imaging on the values of l_c.

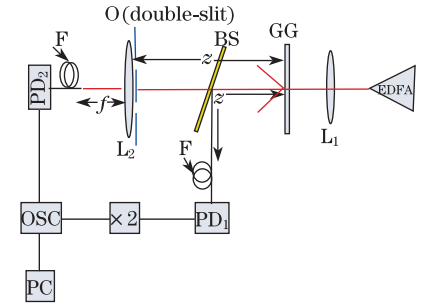

Fig. 3. Novel ghost imaging experimental setup. L_1, L_2: lens; GG: ground glass; BS: beamsplitter; O: object (double-slit); F: fiber; PD: photodiode; OSC: oscilloscope; PC: computer. The intensity acquired by PD_1 is calculated twice for the third-order ghost imaging.

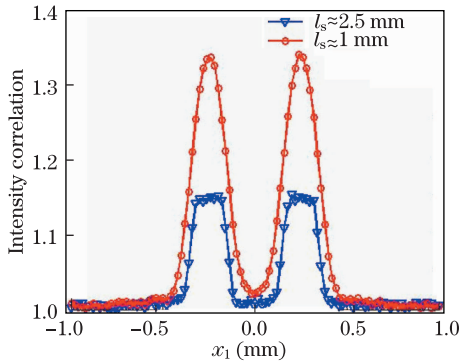

Fig. 4. Reconstructed images obtained by the third-order ghost imaging with different laser diameters on the ground glass.

In conclusion, we theoretically and experimentally show the performance of the third-order ghost imaging with a second-order intensity correlation. The resolution and visibility of the image obtained using the third-order ghost imaging are determined by the optical transverse coherent length l_c located on the detection plane. The resolution is inversely proportional to l_c, whereas the visibility is proportional to l_c. Hence, similar to that observed in the second-order ghost imaging, the tradeoff between the resolution and visibility of images obtained by the third-order ghost imaging continues to exist. The resolution of third-order ghost imaging is the same as that of the second-order ghost imaging, and the visibility can be dramatically enhanced in the third-order ghost imaging under the same optical transverse coherent length. Finally, a third-order ghost imaging experimental setup is proposed and investigated, in which the same second-order correlation is used. This setup can be used for desired-order ghost imaging.

One of the authors, B. Cao, acknowledges the support from the China Scholarship Council.

References

1. R. Hanbury Brown and R. Q. Twiss, Nature **177,** 27 (1956).
2. M. Born and E. Wolf, *Principles of Optics* (Cambridge University Press, Cambridge, 1999).
3. B. Cao and C. Zhang, Opt. Lett. **35,** 2091 (2010).

4. G. Ying, H. Liu, Q. Wei, and S. Han, Acta Opt. Sin. (in Chinese) **29,** 2786 (2009).
5. S. He, X. Shen, H. Wang, W. Gong, and S. Han, Acta Opt. Sin. (in Chinese) **30,** 3332 (2010).
6. T. B. Pittman, Y. H. Shih, D. V. Strekalov, and A. V. Sergienko, Phys. Rev. A **52,** R3429 (1995).
7. J. Lin and J. Cheng, Acta Opt. Sin. (in Chinese) **30,** 2912 (2010).
8. G. Scarcelli, V. Berardi, and Y. Shih, Phys. Rev. Lett **96,** 063602 (2006).
9. J. Liu and Y. Shih, Phys. Rev. A **79,** 023819 (2009).
10. M. Zhang, Q. Wei, X. Shen, Y. Liu, H. Liu, J. Cheng, and S. Han, Phys. Rev. A. **75,** 021803 (2007).
11. H. Liu and S. Han, Opt. Lett. **33,** 824 (2008).
12. A. Gatti, M. Bache, D. Magatti, E. Brambilla, F. Ferri, and L. A. Lugiato, J. Mod. Opt. **53,** 739 (2006).
13. Y. Cai and F. Wang, Opt. Lett. **32,** 205 (2007).
14. X.-H. Chen, Q. Liu, K.-H. Luo, and L.-A. Wu, Opt. Lett. **34,** 695 (2009).
15. Y. Bai and S. Han, Phys. Rev. A **76,** 043828 (2007).
16. D.-Z. Cao, J. Xiong, S.-H. Zhang, L.-F. Lin, L. Gao, and K. Wang, Appl. Phys. Lett. **92,** 201102 (2008).
17. I. N. Agafonov, M. V. Chekhova, T. Sh. Iskhakov, and A. N. Penin, Phys. Rev. A **77,** 053801 (2008).
18. K. W. C. Chan, M. N. O'Sullivan, and R. W. Boyd, Opt. Lett. **34,** 3343 (2009).
19. Goodman, *Statistical Optics* (Wiley-Interscience, New York, 2000).